Efficient Bulk Heterojunction Solar Cells with Poly[2,7-(9,9-dihexylfluorene)-alt-bithiophene] and 6,6-Phenyl C61 Butyric Acid Methyl Ester Blends and Their Application in Tandem Cells

Dewei Zhao,[†,‡,§] Weihua Tang,*[,∥] Lin Ke,[‡] Swee Tiam Tan,[§] and Xiao Wei Sun*[,†]

School of Electrical and Electronic Engineering, Nanyang Technological University, Nanyang Avenue, Singapore 639798, Singapore, Institute of Materials Research and Engineering, ASTAR (Agency for Science, Technology and Research), 3 Research Link, Singapore 117602, Singapore, Institute of Microelectronics, ASTAR (Agency for Science, Technology and Research), 11 Science Park Road, Science Park II, Singapore 117685, Singapore, and College of Chemical Engineering, Nanjing University of Science and Technology, Nanjing 210094, People's Republic of China

ABSTRACT We present herein efficient bulk heterojunction (BHJ) solar cells via mixing poly[2,7-(9,9-dihexylfluorene)-*alt*-bithiophene] (F6T2) and 6,6-phenyl C61 butyric acid methyl ester (PCBM) with variable weight ratios. The photo-physics and morphology of F6T2:PCBM blend films and the electrical characteristics of their corresponding single cells were studied in details by changing PCBM concentration. The complete photoluminescence quenching of F6T2 emission occurs with only a small fraction of PCBM blended, demonstrating effective photoinduced charge transfer between F6T2 and PCBM. Morphology images from atomic force microscopy and scanning electron microscopy (SEM) reveal that the phase separation in F6T2:PCBM blend films becomes pronounced with the increase of PCBM concentration, resulting in the increased fill factor from 25.2% (1:1) to 56.9% (1:6). A SEM image also shows the phase separation is within the range of 10 − 20 nm. With the optimized F6T2:PCBM weight ratio (1:2), the single cell exhibits a highest power conversion efficiency of 2.46% due to the balance of light absorption and charge transport. Finally, the polymer-small molecule tandem cells are constructed using F6T2:PCBM BHJ as the bottom cell and copper phthalocyanine (CuPc):fullerene (C_{60}) as the top cell. The open-circuit voltage (V_{oc}) of tandem cell (1.27 V) is equal to the summation of the V_{oc} values of the bottom cell (0.86 V) and the top cell (0.43 V).

KEYWORDS: organic solar cell • tandem cell • bulk heterojunction

1. INTRODUCTION

Conjugated polymer-based solar cells that convert solar light directly into electricity have been extensively investigated in the past decades. The power conversion efficiency (PCE) of polymer solar cells (PSCs) has recently achieved 5% or more in bulk heterojunction (BHJ) structure, where a photoactive layer is casted from a mixture solution of polymeric electron donors (D) and soluble fullerene-based electron acceptor (A) and sandwiched between two electrodes with different work functions (1, 2). The current workhorse polymeric donors are poly(3-hexylthiophene) (P3HT) and PPVs, whereas fullerene and its derivatives like 6,6-phenyl C61 butyric acid methyl ester (PCBM) are widely employed as the electron acceptors.

In prediction, the efficiency of PSCs can be further increased to 10% by designing new materials (3) and to 15% by exploring efficient tandem structure (4) to address the key issues associated with the light absorption and photoinduced charge transfer and transport. The light absorption can be strengthened by either developing low bandgap polymers (5–7) or using a thick active layer; however, the short exciton diffusion length and relatively low charge mobility in organic semiconductors limit the thickness within 100 nm around. Efficient charge transport in D−A blend film can be facilitated by nanoscale bicontinuous pathways, which also increases the exciton dissociation efficiency by decreasing exciton diffusion distance and increasing the D−A interfacial areas (8–10). It has been demonstrated that the charge transfer from the lowest unoccupied molecular orbital (LUMO) of the donor to the LUMO of the acceptor is extremely fast (−45 fs) (11). This charge transfer is related to the LUMO difference of acceptor and donor, described as LUMO (D)−LUMO (A), determining the driving force for exciton dissociation at the interfaces (12–14). Therefore, for efficient exciton dissociation, such a D−A LUMO difference is required to be at least larger than the exciton binding energy of polymers (typically between 0.1 and 2 eV) (15). On the other hand, the difference between the highest occupied molecular orbital (HOMO) of the donor and LUMO of the acceptor is another important factor, described as HOMO (D)−LUMO (A), on which open-circuit voltage (V_{oc}) is dependent (16). In addition, the V_{oc} is

* To whom correspondence should be addressed. E-mail: exwsun@ntu.edu.sg (X.W.S.); whtang@mail.njust.edu.cn (W.H.T.).
Received for review November 24, 2009 and accepted February 12, 2010
[†] Nanyang Technological University.
[‡] Institute of Materials Research and Engineering, ASTAR.
[§] Institute of Microelectronics, ASTAR.
[∥] Nanjing University of Science and Technology.
DOI: 10.1021/am900823b

also considered to be determined by the work function difference of two electrodes in the metal−insulator−metal (MIM) device (17). Hence, a conjugated polymer donor with suitable energy levels is necessary to maintain a relatively large V_{oc} and obtain efficient charge transfer, contributing to the photocurrent generation and the overall device performance. Furthermore, the performance of BHJ-based PSCs strongly depends on the nanoscale morphology in the active layers. The phase separation occurring in polymer:PCBM blend (10) is determined to a great extent by the solvents used (18–21), the weight ratios of polymer donor to fullerene (8, 22), the concentration of the blend solution (9), and postannealing treatment (1, 23, 24).

A conjugated polymer poly(9,9-dihexylfluorene)-*alt*-bithiophene) (F6T2) has been reported, giving rise to a PCE of 2.7% in the device with a F6T2:PCBM weight ratio of 1:4 (25). Recently, we have reported a detailed study on the thermal and hole-transporting properties of poly[2,7-(9,9-dihexylfluorene)-*alt*-bithiophene] (F6T2) (26), and its photovoltaic performance of BHJ solar cells, consisting of F6T2 as the donor and PCBM as the acceptor with a weight ratio of 1:3 and exhibiting a PCE of 2.4%. Obviously, the weight ratio in such F6T2-based PSCs is as crucial as that in other donor polymer blends, such as P3HT:PCBM (8, 10), MDMO:PPV:PCBM (9, 10), correlated with the phase separation in the two components.

However, thus far, there is still a lack of a detailed study on the influence of the weight ratio of F6T2 to PCBM on the blend morphology and their relation with the device performance. Therefore, this necessitates a comprehensive optimization for this blend based PSCs. As an extension of our previous works, we herein report a more complete solid-state photophysical and morphological characterization of F6T2:PCBM blends with variable weight ratios, and their corresponding single cells are also compared for achieving an optimal efficiency. It is found that a large LUMO difference between F6T2 and PCBM is beneficial to provide enough driving force for the charge transfer at the interface, demonstrated by the complete photoluminescence (PL) quenching of F6T2 with only a little PCBM added. Moreover, in order to further improve the device performance, tandem or stacked structure, consisting of two or more optically and electrically connected cells with complementary absorbers in each cell, is believed to be an effective approach (27, 28). On the basis of the absorption of F6T2 in the short wavelength range, it is used as a bottom cell to implement a polymer-small molecule tandem solar cell. Upon the insertion of an ultrathin Ca in the Al/MoO_3 intermediate layer, the V_{oc} (1.27 V) of the tandem device obtained is the exact summation of those of both sub cells.

2. EXPERIMENTAL SECTION

Device Fabrication. All devices were fabricated on indium tin oxide (ITO) coated glass substrates with a sheet resistance of 20 Ω/square. The substrates were cleaned in an ultrasonic bath with detergent, deionied-water, acetone, and isopropyl alcohol successively for 15 min. After being dried in a laboratory oven, the ITO surfaces were treated by oxygen plasma for 5 min. F6T2 was synthesized as reported (29) and PCBM was purchased from Nano-C. F6T2 and PCBM were dissolved separately in chlorobenzene with 20 mg/mL and stirred at 60 °C for 1 day. They were then mixed together with designated weight ratios. PEDOT:PSS (Baytron P 4083), filtered with 0.45 μm filter syringe, was first spin-coated onto precleaned ITO-glass with a thickness of 40 nm, and baked at 125 °C for 30 min. Subsequently, the substrates were moved into a glovebox filled with N_2 (H_2O < 0.1 ppm and O_2 < 0.1 ppm). For single cells, the active layer was fabricated by spin-coating the blend solution onto PEDOT:PSS coated substrates. Ca (20 nm)/Ag (80 nm), Au (80 nm), Ag (80 nm) cathodes were thermally deposited on the top of the active layer under a vacuum of 2.0×10^{-4} Pa, where Al (100 nm) cathode was deposited by E-beam evaporation. For tandem device, the bottom active layer was prepared, followed by the fabrication of intermediate layer Ca/Al/MoO_3, deposited by thermal and E-beam evaporation. Then, copper phthalocyanine (CuPc), fullerene (C_{60}), and bathophenanthroline (BPhen) were deposited sequentially by thermal evaporation to act as the top cell. Finally, the Ag (80 nm) cathode was deposited. The active area was 0.1 cm^2. A series of the devices were repeated and compared three times; and around 90 devices were fabricated in total. For each comparison, the trend exhibits the same.

Characterization. The optical absorption spectra were recorded using UV−vis-NIR scanning spectrophotometer (UV-3101PC). The films used for absorption measurement were fabricated on PEDOT:PSS coated ITO-glass, where ITO/PEDOT:PSS acted as the reference. The photoluminescence (PL) spectra of pure F6T2, PCBM, various F6T2:PCBM blend thin films were measured using Fluorolog-3 spectrofluorimeter, excited by 450 nm light. The samples were prepared on quartz substrates. The thicknesses for all active layers were measured with a surface profiler (Tencor P15). Scanning electron microscopy (SEM) (JSM-5600) and tapping mode atomic force microscopy (AFM) (D5000, Veeco) were used to characterize the surface topography (phase separation and surface roughness) of the spin-coated F6T2:PCBM layers on PEDOT:PSS based ITO glass. The current−voltage (I−V) characteristics were measured with a Keithley 2400 sourcemeter in dark or under 100 mW/cm^2 (AM 1.5G) irradiation of a solar simulator (Solar Light Company Inc.). The incident photon-to-electron conversion efficiencies (IPCEs) (spectral response) of the devices were measured using Oriel Merlin under short-circuit conditions, meanwhile, the tested devices were illuminated by a 200 W xenon lamp light source with a motorized monochromator (Oriel), calibrated against a silicon solar cell.

3. RESULTS AND DISCUSSION

3.1. Energy Level and Optical Properties.

F6T2 was synthesized in the lab with a high molecular weight (M_w) of 52 400 and polydispersity index (PDI) of 1.99 (29). The chemical structures of donor F6T2 and acceptor PCBM used and the device structure are shown in Figure 1. As reported, F6T2 possesses a LUMO of −2.64 eV and HOMO of −5.13 eV, exhibiting a high bandgap of 2.49 eV. Hence, the energy level diagram of the device can be drawn in Figure 2. To obtain good photovoltaic performance, both the differences of HOMO (D)−LUMO (A) and LUMO (D)−LUMO (A) have to be considered. Large HOMO (D)−LUMO (A) difference is beneficial to a high V_{oc}. LUMO energy matching of donor and acceptor can supply sufficient driving force for exciton separation (12–14). In Figure 2, a large LUMO offset of 1.06 eV is observed (LUMO of PCBM: −3.7 eV (30)), which is significantly larger than the exciton binding energy in F6T2.

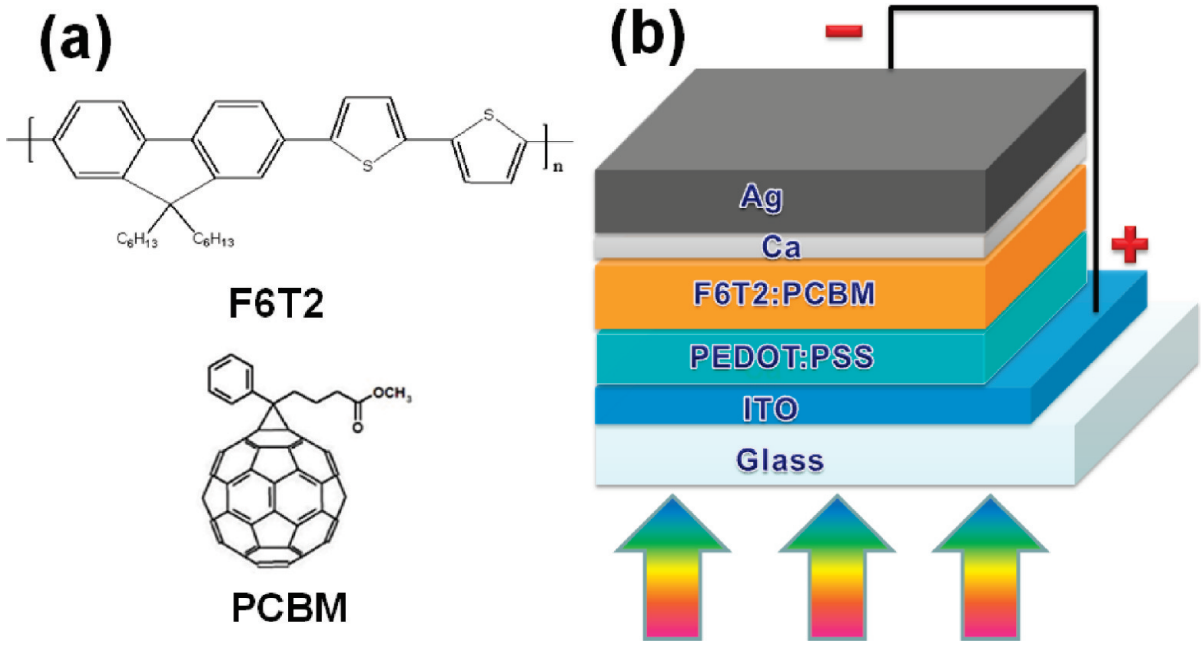

FIGURE 1. (a) Chemical structures of donor F6T2 and acceptor PCBM. (b) Structure of OSC.

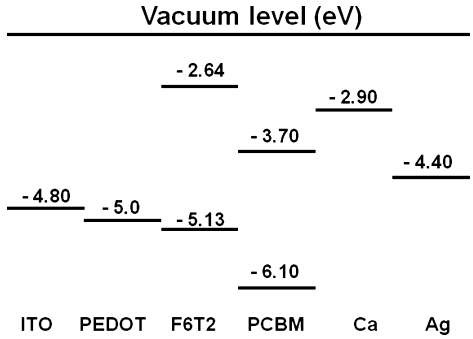

FIGURE 2. Energy level diagram of F6T2:PCBM-based PSC.

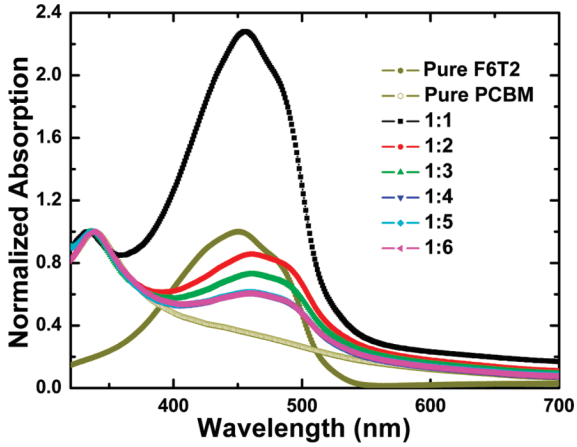

FIGURE 3. Normalized absorption spectra of pure F6T2, pure PCBM, and F6T2:PCBM blend films with different weight ratios.

Therefore, photoinduced charge transfer process from F6T2 to PCBM is favored.

Figure 3 shows the normalized absorption spectra of pure F6T2, pure PCBM, and blend F6T2:PCBM films with different weight ratios. The absorption spectrum of pure F6T2 film displays one main peak located at 450 nm and one slightly weak shoulder at 480 nm, covering an absorption range from 350 to 520 nm, comparable to those of PPV or its derivatives (31), but narrower than that of P3HT (2). Because the absorption range of F6T2 is relatively narrow, a small region of the solar spectrum is covered. It has to be pointed out that only 30% of the photons in the whole solar spectrum (AM1.5G) have an energy higher than 1.9 eV (32). Therefore, this F6T2:PCBM blend (2.49 eV bandgap) is able to absorb only a small fraction of solar light. For F6T2:PCBM blend in Figure 3, two peaks are distinguished, i.e., one peak at ~335 nm stems from PCBM and the other one at ~450 nm represents the contribution from F6T2. Obviously, the addition of PCBM results in a red-shifted F6T2 absorption with the absorption band edge extending to 600 nm. For the F6T2:PCBM (1:1) film, there exists a strong absorption of pristine F6T2, two times higher than that of PCBM. Further increasing PCBM, however, results in a gradual decrease in the F6T2 absorption intensity in comparison with parent F6T2. The absorption intensities of F6T2 level off when the weight ratio of F6T2:PCBM changes to 1:4, 1:5, and 1:6. This is reasonable when considering that conjugated polymer donors serve as the main absorber for the solar photon flux and also as the hole transporting phase.

To investigate the effect of the PCBM concentration on the excited-state charge transfer, steady-state PL measurements were employed for F6T2:PCBM blend films with different weight ratios (pure F6T2, 1:0.5, 1:1, 1:2, and 1:5) and their corresponding normalized PL spectra are shown in Figure 4. To detect PL emission from F6T2, the blend films were excited with a wavelength of 450 nm (the maximum absorption peak of pure F6T2 shown in Figure 3). The PL emission of pure F6T2 film is mainly located at 560 nm, exhibiting a relatively narrow emission width (Figure 4). At a F6T2:PCBM weight ratio of 1:0.5, the PL emission from F6T2 dramatically decreases by over 99% of its emission quenched by the addition of PCBM. As the F6T2:PCBM

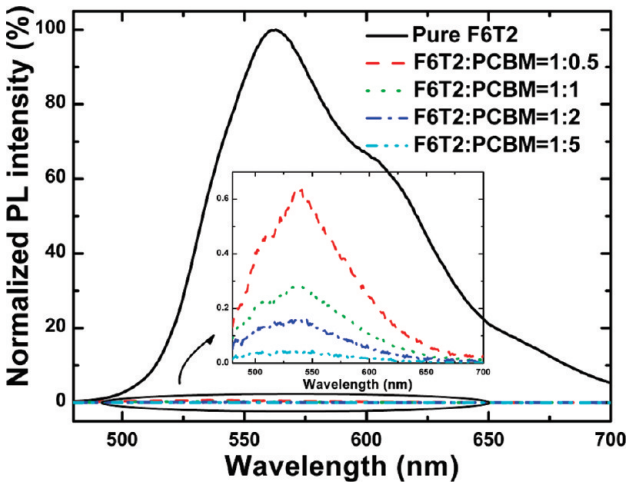

FIGURE 4. Normalized PL spectra of pure F6T2 and F6T2:PCBM (1:0.5, 1:1, 1:2, and 1:5) blend films. All the films were excited at the wavelength of 450 nm.

weight ratio changes to 1:2, the PL emission from F6T2 is further reduced to 0.15% of the original level, indicating the effective fluorescence quenching of F6T2 by PCBM, as similar behavior observed in P3HT:PCBM (33) and MDMO-PPV:PCBM (34, 35) systems. Because the overlap between the PL spectrum of F6T2 and the absorption spectrum of PCBM is rather small, the resonance energy transfer between them can be neglected (36). Therefore, it is the charge transfer between F6T2 and PCBM that leads to the PL quenching with the photogenerated exciton dissociated into electrons and holes before luminescence can occur. From the quenched PL spectra, there exists a slight blue-shift for F6T2 emission, which can be explained by the origin of the residual emission from increasingly short-lived F6T2 excitations (37), or the spectrum superposition of the residual F6T2 emission and the increased PCBM emission. In our F6T2:PCBM system, except for the large LUMO offset of 1.06 eV, the charge-transfer state has a HOMO (D) and LUMO (A) difference of 1.43 eV, smaller than the exciton energy of F6T2 (around 2 eV), which guarantees an energetically favorable charge transfer (15). Thus, the exciton can be efficiently dissociated at the interface under photoexcitation.

3.2. Effect of Weight Ratios on Morphology and Device Performance. Morphology of the BHJ active layer plays a crucial role in the performance of PSCs (8–10, 38). Therefore, we have performed AFM and SEM measurements to investigate the influence of the amount of PCBM in the F6T2:PCBM blends on the morphological differences and phase separation. Considering the real device structure, the films used for measurement were fabricated onto PEDOT:PSS coated ITO-glass substrates. Figure 5 shows the tapping mode AFM images of F6T2:PCBM BHJ active layers with different weight ratios. It can be seen that all the active layers have a rather smooth surface with a root-mean-square (rms) surface roughness less than 1 nm. The active layers for the F6T2:PCBM weight ratios of 1:1, 1:2, and 1:3 display a slightly decreased surface roughness of 0.516 nm (Figure 5a), 0.485 nm (Figure 5b), and 0.439 nm (Figure 5c), respectively. However, with a further increase in PCBM concentration, a small increase in the rms roughness of the active layer for the F6T2:PCBM weight ratios of 1:4 (0.491 nm), 1:5 (0.544 nm), and 1:6 (0.599 nm) samples is observed, as shown in Figure 5d–f, respectively. This could be attributed to PCBM aggregation caused by the high PCBM concentration (10).

Figure 6 shows the SEM images of F6T2:PCBM BHJ active layers with different weight ratios. The pristine F6T2 exhibits no phase separation at all (Figure 6a). When the weight ratio of F6T2:PCBM is 1:2, the phase separation between F6T2 and PCBM domains occurs, though not quite clear (Figure 6b). For other weight ratios, the phase separation becomes more pronounced (landlike areas appear in Figure 6c,d), similar to the observed morphology in F6T2:PCBM (1:3) films (26). It should be noted that the phase separation in our F6T2:PCBM blend is formed during the spin-coating process without any annealing treatments, not like that in P3HT:PCBM systems (8, 10). The well-separated phases in F6T2:PCBM blends would contribute to good photovoltaic performance in such devices (discuss later). Interestingly, the phase separation in the F6T2:PCBM (1:4, Figure 6c) active layer confirms the nanoscale F6T2 and PCBM domains with dimensions of 10–20 nm, which is suitable for efficient exciton dissociation (10, 38).

Figure 7 shows the comparison of the $I-V$ characteristics of the F6T2:PCBM PSCs with different weight ratios under 100 mW/cm^2 illumination. Although the PL quenching is rather complete at the F6T2:PCBM weight ratio of 1:1 (Figure 4), the short-circuit current density (J_{sc}) and fill factor (FF) of the corresponding device are only 1.19 mA/cm^2 and 25.2%, respectively, which are possibly caused by the insufficient PCBM domains for the charge transport pathway. When the weight ratio of F6T2:PCBM changes to 1:2, the J_{sc} of the device is significantly increased to 5.2 mA/cm^2. Further increase in PCBM concentration leads to a slight reduction of J_{sc}, probably due to mismatched electron transport mobility of PCBM and the hole transport mobility of F6T2 (26) and also reduced light absorption by F6T2 (Figure 3). In contrast, the FF increases significantly from 25.2 to 56.9% as the weight ratio of F6T2:PCBM changes from 1:1 to 1:6. As a consequence, despite the fine quenching of F6T2 by only a small amount of PCBM (Figure 4), the efficient charge transport is still influenced by the PCBM volume. It can imagine that F6T2:PCBM (1:1) blend possesses less efficient charge transport, as proved by a rather low FF. For F6T2:PCBM (1:2) blend, FF of the device is still relatively low (53.1%), mainly because of insufficient fullerene percolated pathway. When the PCBM concentration increases further, FF increases accordingly (56%), indicating the improvement of the charge transport. The increase in FF is guaranteed by the relatively high hole mobility (ca. 8.4×10^{-5} cm^2/(V s) at 310 K and 2.5×10^5 V/cm) (26) and is directly associated with the presence of PCBM crystals in the blends and the high probabilities of electrons to escape beyond the capture radius (39). As a consequence, the increase of the PCBM concentration results in a reduced J_{sc}, but significantly improved FF (competitive effect).

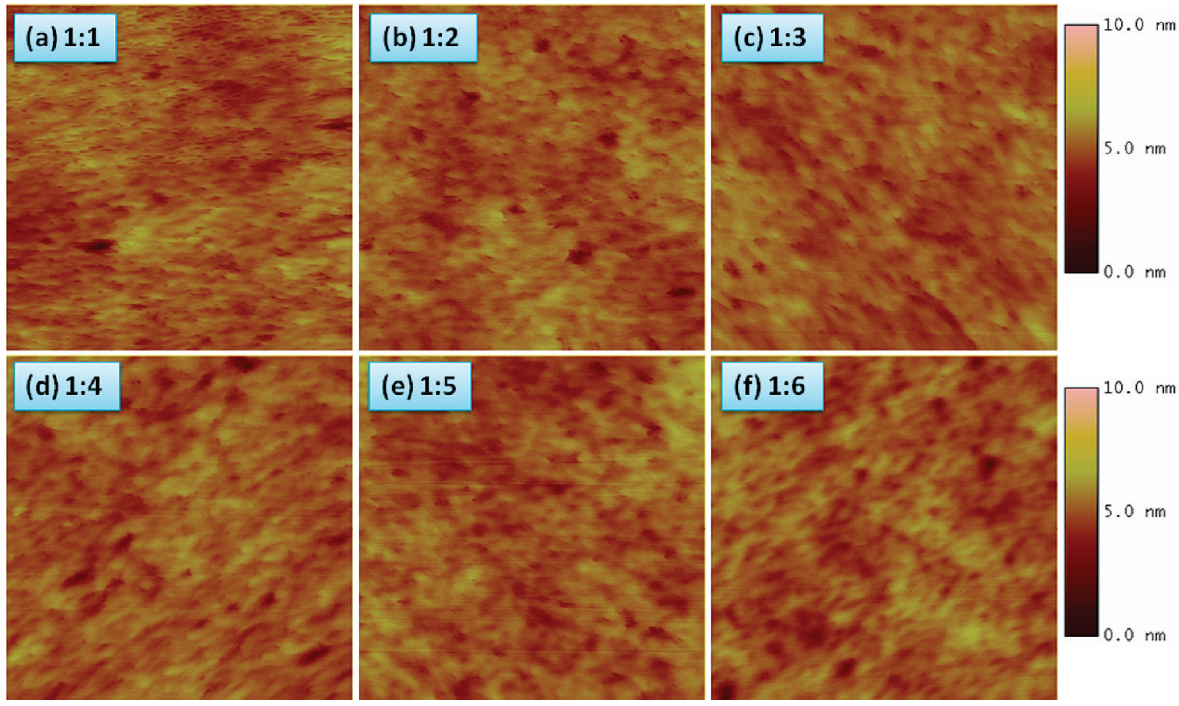

FIGURE 5. Tapping mode AFM height images of F6T2:PCBM BHJ active layers with different weight ratios: (a) 1:1, (b) 1:2, (c) 1:3, (d) 1:4, (e) 1:5, and (f) 1:6. For all images, the height-scale is 10 nm and scan size is 2 × 2 μm^2.

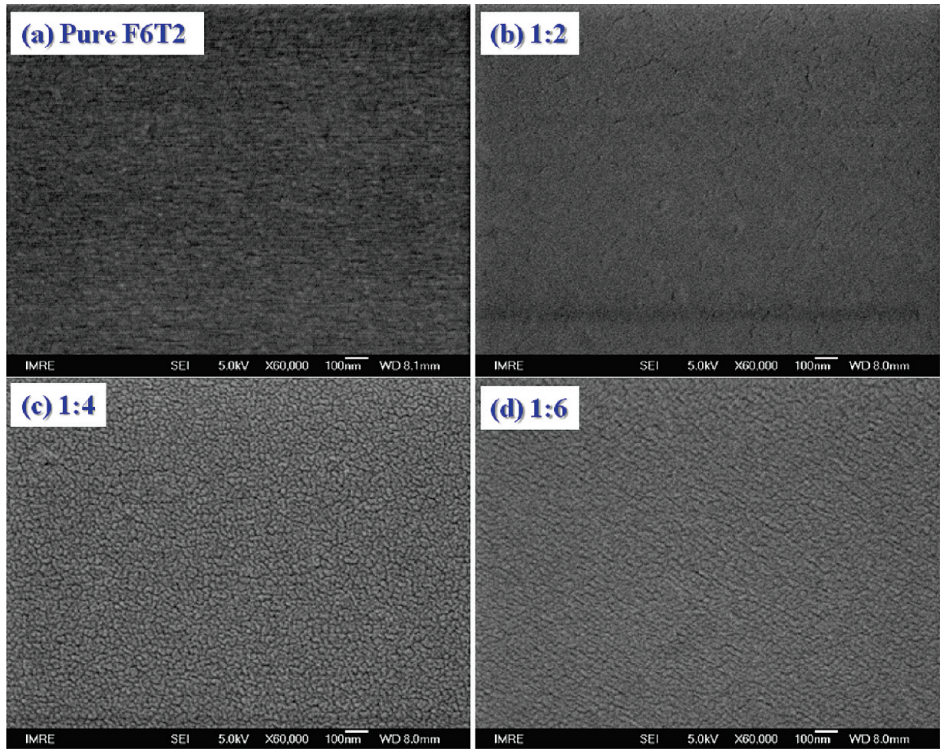

FIGURE 6. SEM images of F6T2:PCBM BHJ active layers with different weight ratios of (a) pure F6T2, (b) 1:2, (c) 1:4, and (d) 1:6.

The V_{oc} is believed to be determined by either the difference of donor HOMO and acceptor LUMO (16) or the work function difference of the electrodes (17). In our F6T2:PCBM devices, the V_{oc} remains around 0.87 V for most devices except the one with the F6T2:PCBM weight ratio of 1:1 (0.99 V), as shown in Figure 7b. The high concentration of F6T2 leads to a relatively higher V_{oc}, similar to other conjugated polymer-fullerene systems (31). As a result, the V_{oc} of F6T2:PCBM cells is not very sensitive to their weight ratios in the blend. To clarify the origin of the V_{oc} in the F6T2:PCBM system, we used different metals as the cathode. The results in the inset of Figure 7a show only a slight variance of V_{oc} (Ca/Ag: 0.89 V; Al: 0.85 V; Ag: 0.82 V; Au: 0.90 V), indicating the independence of the produced V_{oc} on the work

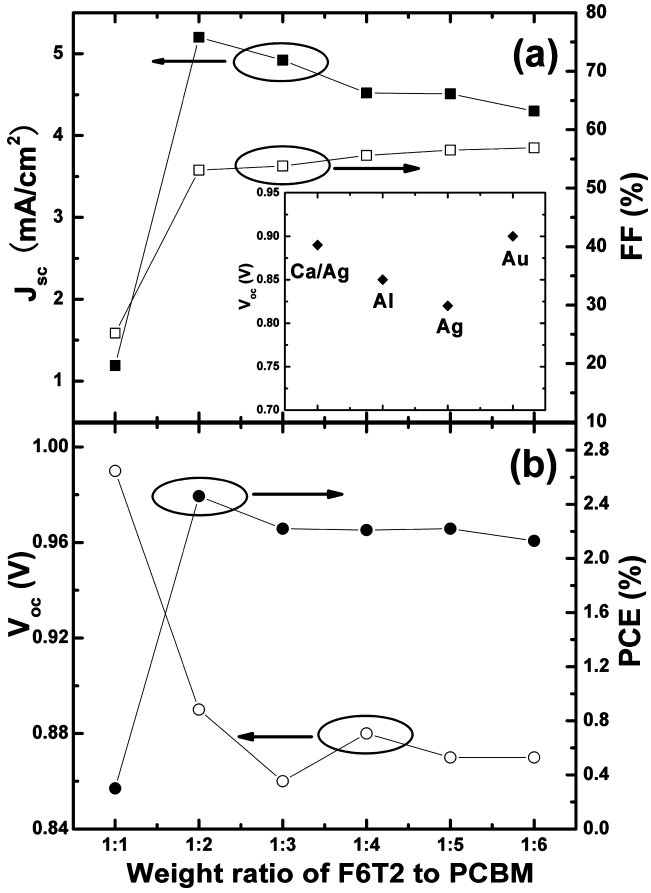

FIGURE 7. Comparison of the $I-V$ characteristics of F6T2:PCBM based polymer solar cells with different weight ratios under 100 mW/cm^2 illumination. (a) J_{sc} (closed square) and FF (open square); (b) V_{oc} (open circle) and PCE (closed circle). The inset in Figure 7a shows the dependence of the V_{oc} of F6T2:PCBM (1:5) devices on the cathode metals used.

function differences of the electrodes. Therefore, the V_{oc} depends on the difference of donor HOMO and acceptor LUMO in our F6T2:PCBM system, which is slightly smaller than the estimated value of 1.13 V (3). Overall, except for the device with the F6T2:PCBM weight ratio of 1:1, the PCE is slightly decreased from 2.46% for the device with the F6T2:PCBM weight ratio of 1:2 to around 2.2% for the devices with other F6T2:PCBM weight ratios.

Additionally, the contribution of each component to the photocurrent generation can be revealed from the IPCE spectra as well. The IPCE spectra of devices with different F6T2:PCBM weight ratios are presented in Figure 8. These spectra are nearly identical with the F6T2 absorption spectrum, giving direct evidence that the excitons are mainly formed in F6T2 phase and there is efficient photoinduced charge transfer between F6T2 and PCBM (36). In other words, for our F6T2:PCBM system, the light is mainly absorbed by the F6T2 phase, and the role of PCBM is to act as the electron acceptor and electron transport material. There are two peaks at 350 and 450 nm originating from PCBM and F6T2, respectively, and the spectral response of these devices primarily covers a range from 320 to 550 nm. The contribution from PCBM (350 nm) is enhanced with the increase of PCBM concentration (inset in Figure 8). However,

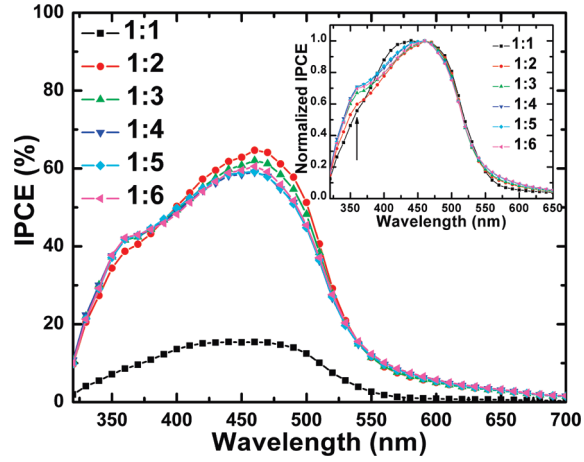

FIGURE 8. IPCE spectra of the devices with different F6T2:PCBM weight ratios. The inset shows their corresponding normalized IPCE spectra.

these IPCE spectra are rather narrow, compared to other conjugated polymer/PCBM based PSCs, which are caused by the narrow absorption range of F6T2. Therefore, the PCEs of these devices are not as high as that of other polymer/PCBM-based devices, though the maximum value of IPCE reaches 65% at 450 nm.

3.3. Application of F6T2:PCBM in Tandem Cell. Organic semiconductors with complementary absorption spectra are essential to construct tandem organic solar cells (27). Currently, P3HT:PCBM BHJ is the most commonly used bottom cell; however, it has a certain spectral overlapping with the top cells made of CuPc:C_{60} (40) or PCPDTBT:PCBM (28). Hence, wide bandgap materials absorbing high energy photons below 600 nm are promising and potential to be applied in tandem devices. The F6T2:PCBM blend is a good choice to meet this requirement. Consequently, we introduced this F6T2:PCBM BHJ as the bottom cell to implement a polymer–small molecule tandem organic solar cell, where small molecule CuPc:C_{60} acts as the top cell. Previously, we have developed an effective and functional intermediate layer of Al(1 nm)/MoO_3(15 nm) in both polymer-small molecule and solution-processed organic solar cells (40, 41). Accordingly, a modified intermediate layer is designed to be Ca/Al/MoO_3(15 nm) here. The resulting structure of the tandem cell is ITO/PEDOT(40 nm)/F6T2:PCBM(50 nm)/intermediate layer/CuPc(20 nm)/C_{60}(40 nm)/BPhen(8 nm)/Ag(80 nm). For comparison, the bottom and top single cells were fabricated in the same run as the tandem cell, with the structures of ITO/PEDOT(40 nm)/F6T2:PCBM(50 nm)/Ca(20 nm)/Ag(80 nm) and ITO/MoO_3(15 nm)/CuPc(20 nm)/C_{60}(40 nm)/BPhen(8 nm)/Ag(80 nm), respectively.

Figure 9a shows the absorption spectra of the bottom, top, and tandem films. It is evident that there is nearly no overlapping between the main absorption ranges of F6T2:PCBM (350–500 nm) and CuPc/C_{60} (550–750 nm) films, exhibiting complementary absorption spectra. The absorption spectrum of the tandem film with Al(1 nm)/MoO_3(15 nm) intermediate layer added corresponds to a simple superposition of features from the absorption spectra of the bottom and top films, thus indicating that the enhanced

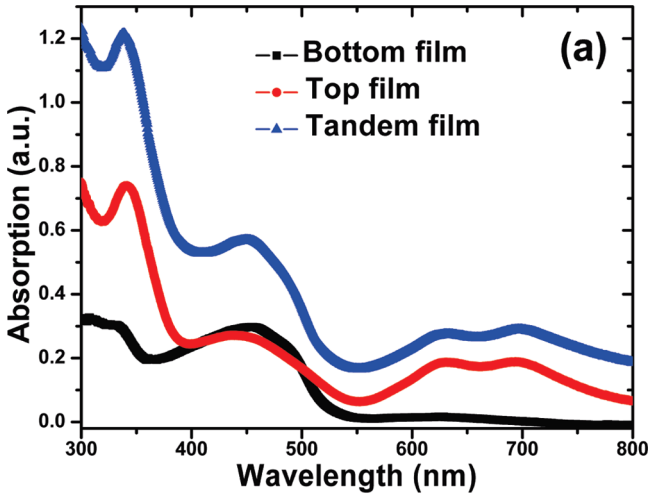

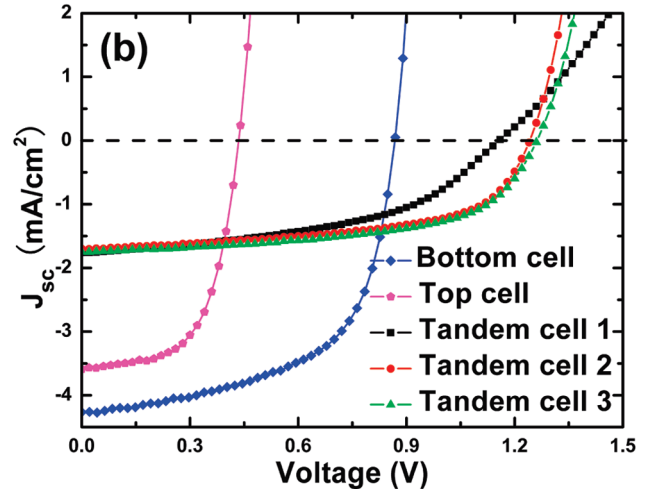

FIGURE 9. (a) Absorption spectra of the bottom film (F6T2:PCBM), top film (CuPc:C_{60}), and tandem film (F6T2:PCBM/Al/MoO_3/CuPc:C_{60}). (b) The $I-V$ characteristics of the bottom cell, top cell, and three tandem cells with different intermediate layers under 100 mW/cm^2 illumination. The bottom cell was made of F6T2:PCBM (1:5) BHJ, and the top cell was made of CuPc and C_{60} bilayer. The $I-V$ curve of the top cell was obtained by fabricating a F6T2:PCBM layer on the glass side of the original top cell. The tandem cell 1, 2, and 3 uses Al(1 nm)/MoO_3(15 nm), Ca(1 nm)/Al(1 nm)/MoO_3(15 nm), and Ca(2 nm)/Al(2 nm)/MoO_3(15 nm) as the intermediate layers, respectively.

absorption is obtainable in such constructed tandem device. Figure 9b shows the $I-V$ characteristics of the single bottom cell, single modified top cell, and three tandem cells with different intermediate layers under 100 mW/cm^2 illumination. Their corresponding data are summarized in Table 1. The bottom cell has a PCE of 2.19% with J_{sc} = 4.27 mA/cm^2, V_{oc} = 0.86 V, and FF = 59.7%. To achieve a performance of the single top cell similar to that of the top cell in the tandem structure, we fabricated a bottom active layer (F6T2:PCBM: 50 nm) onto the glass-side of the single top cell. As a result, the modified top cell has a PCE of 0.93% with J_{sc} = 3.59 mA/cm^2, V_{oc} = 0.43 V, and FF = 60.2%, slightly lower than that of the original top cell without this additional bottom active layer fabricated. It can be observed that the J_{sc} of the tandem cells is only around 1.70 mA/cm^2, reduced to half that of the modified top cell. The low photocurrent of the tandem cell primarily results from the large reduction

Table 1. Summary of $I-V$ Characteristics of the Bottom Cell, Top Cell (Modified), and Tandem Cells with Different Intermediate Layers under 100 mW/cm^2 Illumination[a]

cells	V_{oc}(V)	J_{sc} (mA/cm^2)	FF (%)	PCE (%)
bottom cell	0.86	4.27	59.7	2.19
top cell (modified)	0.43	3.59	60.2	0.93
tandem cell 1 (Al(1 nm)/ MoO_3(15 nm))	1.15	1.76	48.2	0.98
tandem cell 2 (Ca(1 nm)Al(1 nm)/ MoO_3(15 nm))	1.25	1.70	57.7	1.23
tandem cell 3 (Ca(2 nm)Al(2 nm)/ MoO_3(15 nm))	1.27	1.75	57.2	1.27

[a] For testing the similar performance of the single top cell to that of the top cell in the tandem structure, a bottom active layer (F6T2:PCBM = 50 nm) was fabricated onto the glass-side of the single top cell.

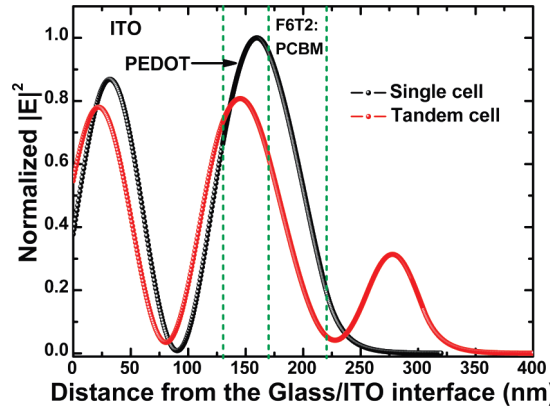

FIGURE 10. Simulated optical field distribution (for 450 nm illumination) in single and tandem cells. The ultrathin Ca and Al in the intermediate layer of tandem cell are neglected in the simulation.

of J_{sc} in the bottom cell because the interference effect is weakened with the top cell stacked, i.e., that the light reflected by cathode (Ag) is decreased largely, especially for the bottom cell. To understand this effect, we simulated the optical field distribution for a single wavelength illumination (450 nm, the maximum absorption peak of F6T2:PCBM blend) in both single and tandem cells (42, 43), as shown in Figure 10. With the top cell stacked, the relative intensity across the F6T2:PCBM active layer is significantly reduced. Moreover, the second interference maxima has shifted to the ITO/PEDOT interface, away from the active layer of the bottom cell, resulting in less exciton generation and low photocurrent in the bottom cell (44). Hence, it has to be pointed out that the complementary absorption of organic semiconductor materials is only one of the prerequisites for the efficiency enhancement in tandem cell, not the determining one. The photocurrent from each subcell in tandem cell is correlated with the light absorption (related to the effective optical field distribution in the photoactive layer). Because the photocurrent extracted from the tandem cell is determined by the smallest photocurrent generated among all subcells stacked in series, a matched photocurrent in all subcells is crucial. This should be realized by optimizing

the thickness and architecture of subcells for a balanced photocurrent.

When the Al(1 nm)/MoO_3(15 nm) intermediate layer is used in tandem cell 1, the V_{oc} is only 1.15 V and the FF of 48.2% is also low. An ultrathin Ca of 1 nm inserted in the existing intermediate layer (tandem cell 2) results in the increase of V_{oc} to 1.25 V, about the sum of the V_{oc} values of both subcells. Meanwhile, the FF is largely increased to 57.7%. Because the work function of Ca (2.9 eV) is lower than the Fermi level of PCBM (4.7 eV), the Ohmic contact is favorable between Ca and PCBM. On the contrary, the rectifying contact is formed between Ca and F6T2, which effectively blocks the hole collection by the cathode of bottom cell, compared with an intermediate layer without Ca layer. Thus, the modified intermediate layer (Ca/Al/MoO_3) functions well as the recombination center of charge carriers. Moreover, the improved contact lowers the series resistance of the tandem device, as shown in Figure 9b. Hence the FF increases significantly.

Overall, these enhanced parameters lead to an improved PCE of 1.23%, higher than that of the top cell (0.93%). With the introduction of a thicker Ca(2 nm)Al(2 nm)/MoO_3(15 nm) intermediate layer, the PCE of tandem cell 3 (1.27%) is slightly improved with a nearly constant J_{sc} of 1.75 mA/cm^2 and slightly increased V_{oc} of 1.27 V.

4. CONCLUSIONS

We have presented efficient F6T2:PCBM-based BHJ PSCs and have demonstrated the potential application in tandem cells. The large LUMO difference between F6T2 and PCBM facilitates the charge transfer and exciton separation, elucidated by the PL quenching of F6T2 with PCBM mixed. The photocurrent and charge transport exhibit strong correlation to the morphology of F6T2:PCBM blends with different weight ratios. The single cell with a F6T2:PCBM (1:2) blend gives rise to the highest J_{sc} and overall efficiency of 2.46%. The results show that the improved charge transport occurs with the increase in PCBM concentration because of the interpenetrating networks induced by the fine phase separation. Optimization of the composite weight ratio reveals the important role played by the morphology for the charge-transport properties of F6T2:PCBM BHJ devices.

Importantly, F6T2:PCBM single cell is further employed as the bottom cell in polymer-small molecule tandem cells by stacking CuPc:C_{60} as the top cell. By inserting an ultrathin Ca into previous Al(1 nm)/MoO_3(15 nm) intermediate layer, the V_{oc} (1.27 V) of the tandem cell approaches the exact summation of those of bottom (0.86 V) and top (0.43 V) cells, indicating that the F6T2:PCBM is preferable to Ca contact without voltage loss across the intermediate layer. The PCE of tandem cell is larger than that of the top cell, but lower than that of the bottom cell. The optimization of this tandem cell may provide an insight for the potential application of F6T2:PCBM single cell.

Acknowledgment. The authors are grateful for the partial financial support from Academic Research Fund (RGM 44/06) of Ministry of Education, Singapore.

REFERENCES AND NOTES

(1) Ma, W. L.; Yang, C. Y.; Gong, X.; Lee, K.; Heeger, A. J. *Adv. Funct. Mater.* **2005**, *15*, 1617.
(2) Reyes-Reyes, M.; Kim, K.; Carroll, D. L. *Appl. Phys. Lett.* **2005**, *87*, 083506.
(3) Scharber, M. C.; Wuhlbacher, D.; Koppe, M.; Denk, P.; Waldauf, C.; Heeger, A. J.; Brabec, C. L. *Adv. Mater.* **2006**, *18*, 789.
(4) Dennler, G.; Scharber, M. C.; Ameri, T.; Denk, P.; Forberich, K.; Waldauf, C.; Brabec, C. J. *Adv. Mater.* **2008**, *20*, 579.
(5) Wienk, M. M.; Turbiez, M. G. R.; Struijk, M. P.; Fonrodona, M.; Janssen, R. A. J. *Appl. Phys. Lett.* **2006**, *88*, 153511.
(6) Zhang, F. L.; Mammo, W.; Andersson, L. M.; Admassie, S.; Andersson, M. R.; Inganas, L.; Ingands, O. *Adv. Mater.* **2006**, *18*, 2169.
(7) Bundgaard, E.; Krebs, F. C. *Sol. Energy Mater. Sol. Cells* **2007**, *91*, 954.
(8) Chirvase, D.; Parisi, J.; Hummelen, J. C.; Dyakonov, V. *Nanotechnology* **2004**, *15*, 1317.
(9) Hoppe, H.; Niggemann, M.; Winder, C.; Kraut, J.; Hiesgen, R.; Hinsch, A.; Meissner, D.; Sariciftci, N. S. *Adv. Funct. Mater.* **2004**, *14*, 1005.
(10) Hoppe, H.; Sariciftci, N. S. *J. Mater. Chem.* **2006**, *16*, 45.
(11) Brabec, C. J.; Zerza, G.; Cerullo, G.; De Silvestri, S.; Luzzati, S.; Hummelen, J. C.; Sariciftci, S. *Chem. Phys. Lett.* **2001**, *340*, 232.
(12) Wang, X. J.; Perzon, E.; Delgado, J. L.; de la Cruz, P.; Zhang, F. L.; Langa, F.; Andersson, M.; Inganas, O. *Appl. Phys. Lett.* **2004**, *85*, 5081.
(13) Wang, X. J.; Perzon, E.; Oswald, F.; Langa, F.; Admassie, S.; Andersson, M. R.; Inganas, O. *Adv. Funct. Mater.* **2005**, *15*, 1665.
(14) Zhang, F. L.; Bijleveld, J.; Perzon, E.; Tvingstedt, K.; Barrau, S.; Inganas, O.; Andersson, M. R. *J. Mater. Chem.* **2008**, *18*, 5468.
(15) Peumans, P.; Yakimov, A.; Forrest, S. R. *J. Appl. Phys.* **2003**, *93*, 3693.
(16) Brabec, C. J.; Cravino, A.; Meissner, D.; Sariciftci, N. S.; Fromherz, T.; Rispens, M. T.; Sanchez, L.; Hummelen, J. C. *Adv. Funct. Mater.* **2001**, *11*, 374.
(17) Parker, I. D. *J. Appl. Phys.* **1994**, *75*, 1656.
(18) Zhang, F. L.; Jespersen, K. G.; Bjorstrom, C.; Svensson, M.; Andersson, M. R.; Sundstrom, V.; Magnusson, K.; Moons, E.; Yartsev, A.; Inganas, O. *Adv. Funct. Mater.* **2006**, *16*, 667.
(19) Chen, F. C.; Tseng, H. C.; Ko, C. J. *Appl. Phys. Lett.* **2008**, *92*, 103316.
(20) Moule, A. J.; Meerholz, K. *Adv. Mater.* **2008**, *20*, 240.
(21) Rispens, M. T.; Meetsma, A.; Rittberger, R.; Brabec, C. J.; Sariciftci, N. S.; Hummelen, J. C. *Chem. Commun.* **2003**, 2116.
(22) Jin, S. H.; Naidu, B. V. K.; Jeon, H. S.; Park, S. M.; Park, J. S.; Kim, S. C.; Lee, J. W.; Gal, Y. S. *Sol. Energy Mater. Sol. Cells* **2007**, *91*, 1187.
(23) Yang, X. N.; Loos, J.; Veenstra, S. C.; Verhees, W. J. H.; Wienk, M. M.; Kroon, J. M.; Michels, M. A. J.; Janssen, R. A. J. *Nano Lett.* **2005**, *5*, 579.
(24) Kim, K.; Liu, J.; Namboothiry, M. A. G.; Carroll, D. L. *Appl. Phys. Lett.* **2007**, *90*, 163511.
(25) Schulz, G. L.; Chen, X. W.; Holdcroft, S. *Appl. Phys. Lett.* **2009**, *94*, 023302.
(26) Tang, W. H.; Chellappan, V.; Liu, M. H.; Chen, Z. K.; Ke, L. *ACS Appl. Mater. Interfaces* **2009**, *1*, 1467.
(27) Hadipour, A.; de Boer, B.; Wildeman, J.; Kooistra, F. B.; Hummelen, J. C.; Turbiez, M. G. R.; Wienk, M. M.; Janssen, R. A. J.; Blom, P. W. M. *Adv. Funct. Mater.* **2006**, *16*, 1897.
(28) Kim, J. Y.; Lee, K.; Coates, N. E.; Moses, D.; Nguyen, T. Q.; Dante, M.; Heeger, A. J. *Science* **2007**, *317*, 222.
(29) Tang, W. H.; Ke, L.; Tan, L. W.; Lin, T. T.; Kietzke, T.; Chen, Z. K. *Macromolecules* **2007**, *40*, 6164.
(30) Shrotriya, V.; Li, G.; Yao, Y.; Chu, C. W.; Yang, Y. *Appl. Phys. Lett.* **2006**, *88*, 073508.
(31) Gunes, S.; Neugebauer, H.; Sariciftci, N. S. *Chem. Rev.* **2007**, *107*, 1324.
(32) Blom, P. W. M.; Mihailetchi, V. D.; Koster, L. J. A.; Markov, D. E. *Adv. Mater.* **2007**, *19*, 1551.
(33) Hwang, I. W.; Moses, D.; Heeger, A. J. *J. Phys. Chem. C* **2008**, *112*, 4350.
(34) Nikitenko, S. L.; Mayorova, J. Y.; Troshin, P. A.; Lyubovskaya, R. N.; Kaplunov, M. G. *Mol. Cryst. Liq. Cryst.* **2007**, *468*, 591.
(35) Dennler, G.; Mozer, A. J.; Juska, G.; Pivrikas, A.; Osterbacka, R.; Fuchsbauer, A.; Sariciftci, N. S. *Org. Electron.* **2006**, *7*, 229.

(36) Wang, P.; Abrusci, A.; Wong, H. M. P.; Svensson, M.; Andersson, M. R.; Greenham, N. C. *Nano Lett.* **2006**, *6*, 1789.
(37) van Duren, J. K. J.; Yang, X. N.; Loos, J.; Bulle-Lieuwma, C. W. T.; Sieval, A. B.; Hummelen, J. C.; Janssen, R. A. J. *Adv. Funct. Mater.* **2004**, *14*, 425.
(38) Chen, L. M.; Hong, Z. R.; Li, G.; Yang, Y. *Adv. Mater.* **2009**, *21*, 1.
(39) Veldman, D.; Ipek, O.; Meskers, S. C. J.; Sweelssen, J.; Koetse, M. M.; Veenstra, S. C.; Kroon, J. M.; van Bavel, S. S.; Loos, J.; Janssen, R. A. J. *J. Am. Chem. Soc.* **2008**, *130*, 7721.
(40) Zhao, D. W.; Sun, X. W.; Jiang, C. Y.; Kyaw, A. K. K.; Lo, G. Q.; Kwong, D. L. *Appl. Phys. Lett.* **2008**, *93*, 083305.
(41) Zhao, D. W.; Sun, X. W.; Jiang, C. Y.; Kyaw, A. K. K.; Lo, G. Q.; Kwong, D. L. *IEEE Electron Device Lett.* **2009**, *30*, 490.
(42) Pettersson, L. A. A.; Roman, L. S.; Inganas, O. *J. Appl. Phys.* **1999**, *86*, 487.
(43) Zhao, D. W.; Liu, P.; Sun, X. W.; Tan, S. T.; Ke, L.; Kyaw, A. K. K. *Appl. Phys. Lett.* **2009**, *95*, 153304.
(44) Moule, A. J.; Bonekamp, J. B.; Meerholz, K. *J. Appl. Phys.* **2006**, *100*, 094503.

AM900823B